Journal Pre-proof

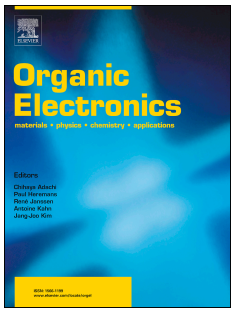

Improving device performance of p-type organic field-effect transistor using butterfly like triarylamines

Ramachandran Dheepika, Anisha Shaji, Predhanekar Mohamed Imran, Samuthira Nagarajan

PII: S1566-1199(19)30595-6

DOI: https://doi.org/10.1016/j.orgel.2019.105568

Reference: ORGELE 105568

To appear in: *Organic Electronics*

Received Date: 5 June 2019

Revised Date: 28 August 2019

Accepted Date: 17 November 2019

Please cite this article as: R. Dheepika, A. Shaji, P.M. Imran, S. Nagarajan, Improving device performance of p-type organic field-effect transistor using butterfly like triarylamines, *Organic Electronics* (2019), doi: https://doi.org/10.1016/j.orgel.2019.105568.

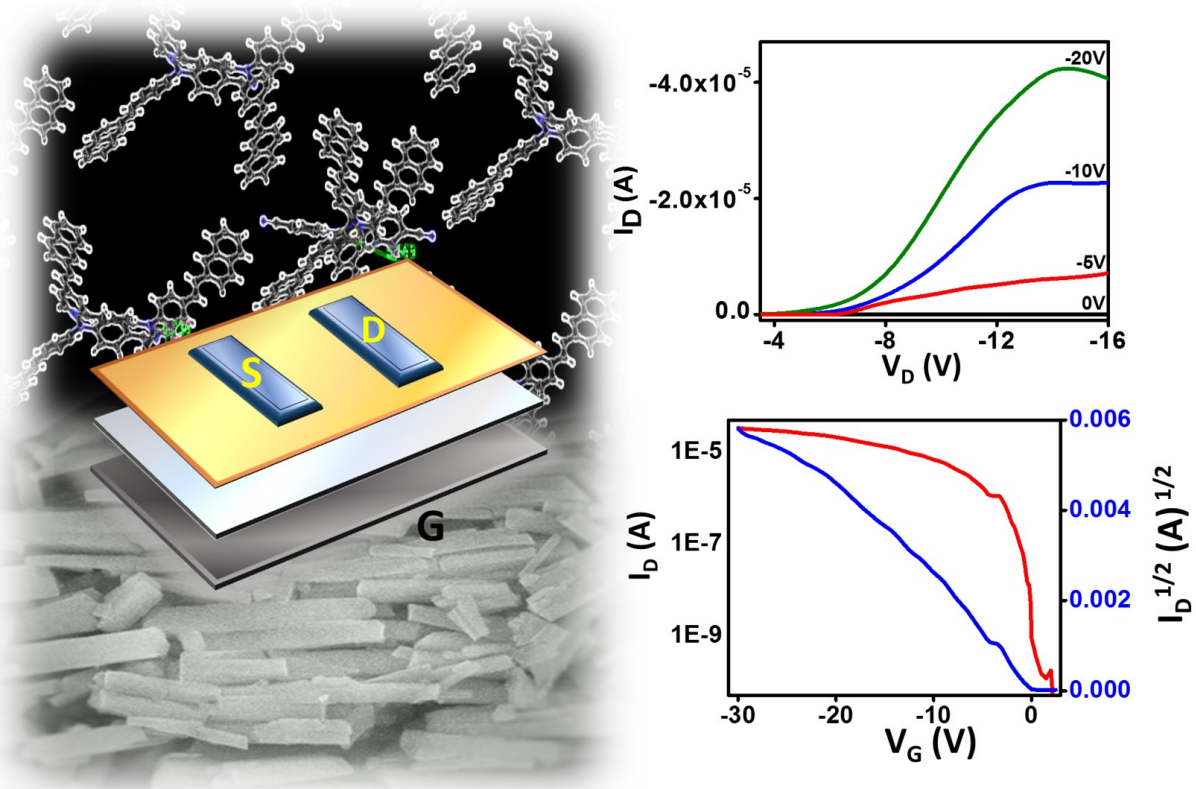
S
D
G
-20V
-10V
-6V
0V
-4.0x10^-5
-2.0x10^-5
0.0
I_D (A)
-4
-8
-12
-16
V_D (V)
1E-5
1E-7
1E-9
I_D (A)
0.006
0.004
0.002
0.000
I_D^1/2 (A)^1/2
-30
-20
-10
0
V_G (V)

Improving Device Performance of *p-type* Organic Field-effect Transistor using Butterfly like Triarylamines

Ramachandran Dheepika, [a] Anisha Shaji, [a] Predhanekar Mohamed Imran, [b] Samuthira Nagarajan*[a]

[a]*Department of Chemistry, Central University of Tamil Nadu, Thiruvarur, India, 600 005.*
[b]*Department of Chemistry, Islamiah College, Vaniyambadi, India, 635 752.*

*Corresponding Author: snagarajan@cutn.ac.in, +91-94430 46272

Abstract

Facile and economic strategy to create a controlled self-structured architecture of semiconducting molecules is very crucial in the accomplishment of carbon electronic devices. A series of new unsymmetrically functionalized butterfly type triarylamines with electron donating/withdrawing substituents were synthesized. Simple and efficient solution based method was used as a successful strategy for OFET with improved characteristics. Binary solvent system with chloroform and toluene (7:3) has improved inter/intra molecular communication in the active layer. The morphology of the films was analysed by SEM reveals the uniform packing. In addition post thermal annealing has enhanced the crystallinity with minimal grain boundaries. HOMO values 5.1 to 5.4 eV obtained from cyclic voltammetry ensure that these molecules can efficiently transport holes. OFET devices were fabricated in bottom gate top contact (BGTC) architecture by spin coating. Molecules exhibited typical *p*-channel transistor behaviour with mobility up to 1 $cm^2 V^{-1}s^{-1}$ with 10^6 $I_{on/off}$ current ratio. Density functional theory (DFT) visualised the packing and interaction of molecules and supported the efficient mobility. Our investigation gives insight into the role of solvents to control the film architecture in solution processing OFET device construction.

Keywords: Solvent engineering, binary solvent system, triarylamines, OFET

1. Introduction

Organic field-effect transistors (OFETs) are being actively studied by organic electronics community due to their facile, cost-effective production [1-2] and their potential application in flexible large area display devices, smart cards and sensors [3-7]. Extraordinary beliefs are placed on solution processable organic small molecules as a gateway towards the real world applications. Because polymer molecules have a large distribution of molecular weight their devices suffers with batch to batch variations [8]. Among many small molecules investigated rubrene, pentacene, and thiophene have excellent OFET characteristics [9-12]. In addition triarylamines (TAAs) are also studied for their applicability in OFET owing to their structure and electronic properties [13-17]. TAA based molecules have inherent advantages including a peculiar geometry, high electron donating and hole transporting ability [18]. Their optoelectronic applications are studied extensively in the past years. However their application towards OFETs are restricted because of their amorphous film forming tendency [19]. Understanding of structure-property relationship remains as the challenge of now-a-days research to outperform their transistor characteristics.

The real life application of OFETs relies on their high performance in terms of mobility, on-off ratio and operational stability. Therefore, recent research focuses on developing the impressive molecular design to improve the molecular assembly and to optimise the film morphology. The aspects related to device performance are scrutinised by a few factors such as molecular self-assembly, thin film morphology, and crystallinity which are regulated by inter and intramolecular interaction. These can be altered and/or improved by different processing methods [20-22]. A few layers of organic semiconductor near dielectric/active layer interface is significantly responsible for carrier movement and influenced by crystallinity. The grain boundaries, which will trap or scatter the charge carriers can be minimised by choosing a suitable fabrication style [23, 24]. Solution processing techniques, such as spin coating, drop casting, inkjet printing are unquestionably easy and economical way to produce crystalline films.

However, controlling the crystallisation to reach ordered thin film remains as the question of research. The anisotropy of the films lead to variation in performance

[25]. Consequently, choice of solvent is an impressive way to regulate the film morphology. Use of additives with solvents for active layer deposition helps to control the crystallization [26]. The crystalline order can be improved by post deposition methods such as solvent vapour annealing and thermal annealing [27-29]. Combination of a low and high boiling solvents result in favourable molecular assembly due to the control in evaporation rate. Low volatile solvents provide sufficient time for supramolecular self-assembly but the residual solvents must be removed by further process. In case of highly volatile solvents the residual solvents can be removed easily but time available for self-assembly is insufficient [25]. Specific proportion of high and low boiling solvents will be the perfect strategy to produce favourable assembly without any further complicated processes.

In this work, we designed and synthesised a series of new TAA molecules with an ethylene spacer and electron withdrawing/donating group to explore their self-assembling tendency towards high performing *p*-channel OFET application. The molecules are designed with an expectation that the unsymmetrical substitution of TAA provides better molecular packing due to unequal electron distribution assisted pi-pi stacking. A simple and proficient solvent engineering strategy to produce crystalline thin film by spin coating method is investigated. The binary solvent system assists the molecule to communicate via inter and intramolecular interactions and produce uniform film. Whereas, the proportion of the solvent helps to change the alignment of the molecules in solution. And a post deposition thermal annealing process to improve the order of the thin film is also scrutinised for high charge carrier mobility. This investigation can give an idea about solvent engineering as a platform to understand solution processing and eventually guides to high performing OFETs.

2. Experimental Section

2.1 Materials

Triphenylamine, dimethyl formamide (DMF), $POCl_3$, potassium iodide, potassium iodate, palladium (II) acetate, and styrenes were purchased from commercial sources

and used as received. Solvents used for synthesis were obtained from Merck; for analysis anhydrous solvents were used.

2.2 Methods

Molecules were characterized by ^{1}H and ^{13}C NMR in a Bruker 400 MHz instrument using $CDCl_3$ as solvent and TMS as internal standard. Thermo Exactiveplus UPHLC – HRMS was used for further confirmation of the molecules. Photophysical properties were analyzed in JASCO UV-NIR spectrophotometer and Perkin Elmer Spectrofluorimeter LS55. CHI electrochemical workstation was utilized to scrutinize the electrochemical behavior (cyclic voltammetry, CV) in a three electrode electrochemical cell. The electrochemical cell was composed of three electrodes; glassy carbon served as working electrode, platinum wire as counter electrode and SCE as reference electrode. The glassy carbon electrode was polished with alumina (1, 0.5 and 0.03 micron successively) before each experiment. TA thermal analyzer was used to study their thermal behavior. Density functional theory, DFT was employed to get insight into geometrical and electronic features of the molecules in ground state. And extended to time dependent density functional theory (TD-DFT) to analyze their excited state. OFET devices were characterized in Keithley 4200 SCS. The topography of the thin films coated from a binary solvent system by spin coating were investigated using Jeol JSM 6390 scanning electron microscope (SEM).

2.3 Synthesis

Precursors **1** and **2** were synthesized according to the literature methods [30-31]. Commercially available triphenylamine underwent Vilsmeier-Haack formylation and followed by iodination. The formyl group was converted into nitrile group by hydroxylamine hydrochloride in presence of DMSO. The precursors were subjected to Heck coupling in presence of palladium catalyst to yield the ethylene bridged triarylamines in good yield. Anhydrous solvents were used for synthesis and purged

with nitrogen for 10 minutes. Detailed spectra of the compounds are given in supplementary information.

2.4 General procedure of Heck coupling reaction

Precursor **1** or **2** (0.95 mmol, 1 equiv.) was dissolved in a mixture of CH_3CN and triethylamine (1:1 ratio) in a flask and purged with nitrogen for 10 minutes. Palladium acetate (10 mol %) was added under nitrogen and stirred at room temperature for 15 minutes. Finally corresponding styrene (2.09 mmol, 2.2 Equiv.) was introduced and temperature raised to reflux, continued for 12 hours. The reaction progress was monitored by thin layer chromatography. After completion of the reaction, filtered through celite and the crude was washed with DCM and extracted. The organic layer was washed twice with water and once with brine solution, dried over Na_2SO_4. The product obtained was purified by column chromatography (SiO_2, 100-200 mesh size) with hexane: ethyl acetate gradient solvent system. Yellow solid was obtained in moderate to good yields.

2.5 Device fabrication and characterization

Bottom gate top contact OFETs are fabricated using heavily n^{++} doped silicon wafer. The wafer was ultrasonically cleaned in acetone and methanol. And followed by a mild piranha solution wash. Then the cleaned wafer was heated up to 1200 °C for 80 minutes to grow silicon dioxide dielectric layer. This thermally grown dielectric layer thickness was ~300 nm. Si wafer served as gate. The compounds were dissolved in a binary solvent mixture composed of chloroform and toluene in 7:3 ratio and sonicated for 20 minutes. Then this solution was spin coated on the SiO_2 dielectric layer at 3200 rpm speed for 45 seconds. The device was then soft baked over a hot plate at 60 °C to get rid of residual solvent. As a post deposition treatment it is thermally annealed at 90 °C for 30 minutes. Finally source and drain contact were made by conductive silver paste to finish the fabrication. The channel length and width were 150 mm and 5 mm respectively. BGTC devices were characterized using

Keithley 4200 SCS analyzer. Typical *p*-channel behavior was observed in the BGTC devices fabricated.

3. Results and Discussion

TAA based new small molecules were designed due to their unusual geometry; where, the unsymmetrical design improves the self-assembly on substrate and consequently upgrade the transistor characteristics. Distinct crystalline alignment of the film produces inspiring π-stacking between the molecules to attain better electronic coupling and promotes mobility. Transistor characteristics greatly depends on the processing methods. Here, the binary solvent system used for active layer deposition is responsible for the morphology. The solution was sonicated, which lead

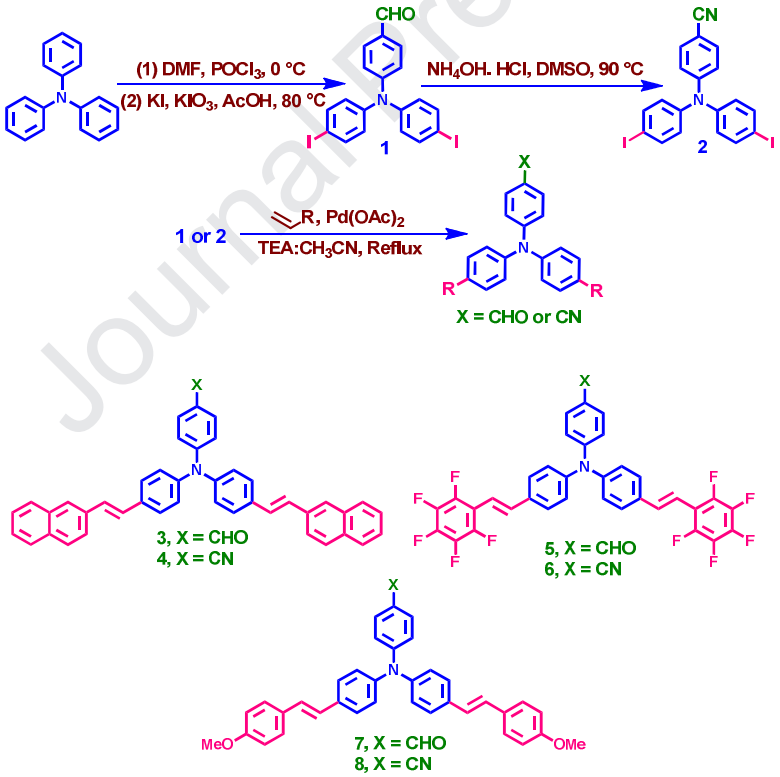

Scheme 1. Sythetic route and structure of compounds **1-8**

to formation of an alignment of molecules in solution and on spin coating process it can produce ordered structure [32]. As post deposition process thermal annealing was performed to improve the order of the crystallinity of the film. Molecules were constructed by Heck coupling reactions under nitrogen atmosphere. Synthetic route and the molecular structure is given in **Scheme 1**.

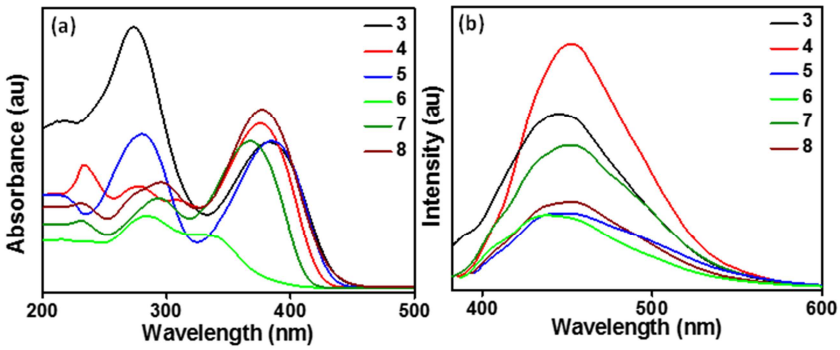

Figure 1. (a) Absorption (b) emission spectra of compounds **3**-**8** in anhydrous dichloromethane

3.1 Photophysical properties

To understand the optoelectronic properties of the synthesized molecules (**1**-**8**), absorption and emission behavior was analyzed in anhydrous dichloromethane (DCM) at 10^{-5} M concentration in room temperature. Corresponding spectral parameters are represented in Table 1 and UV-vis absorption spectra is given in Figure 1 (a). These compounds exhibit two distinct bands: higher energy band corresponds to π-π* transition and lower energy band is attributed to n-π* transitions. According to quantum chemical calculations, this lower energy transitions involves the entire molecule and originated from S_0-S_1 transitions [33]. However, the result reveals that increasing the conjugation improves the overall electron density and lowers the energy of the system leads to red shift irrespective of electron withdrawing

and donating substituents [34]. Except compound **6**, all other nitrile substituted molecules exhibited relatively high absorbance than the corresponding aldehydes. The low absorbing tendency of the compound **6** may be due to the twist created by fluorine with the nitrile in the other arm [33].

Table 1. Photophysical properties of compounds **1**-**8**

Compd. No.	λ_{abs} (nm)		λ_{em} (nm)	Stokes shift (nm)	Absorption coefficient (ε) (10^4 M^{-1} cm^{-1})	Quantum yield, (ϕ)[a]
	λ_1	λ_{max}				
3	273	382	444	69	4.9	0.77
4	277	375	452	77	5.5	0.93
5	280	385	449	63	5.0	0.66
6	283	340	435	94	1.6	0.59
7	294	367	450	84	4.9	0.71
8	296	378	452	54	6.0	0.68

[a] Quantum yield calculated using quinine sulphate as standard.

Emission spectra of the compounds were also analyzed in anhydrous DCM at 10^{-8} M and are shown in Figure 1 (b). The compounds were excited at corresponding absorption λ_{max} and invariably all the compounds exhibited blue emission in the broad region of 380-580 nm [35]. Following the trend of absorption, compounds **3** and **4** exhibited higher intensity among the molecules studied. The electron donating and withdrawing groups may change the excited state geometry of the molecules in polar medium thus the molecule gains twist and rupture the conjugation [36]. Although, for all the compounds emission wavelength is observed to be the same, intensity of emission varies significantly. Quantum yield (**ϕ**) is determined using quinine as standard. All the compounds have very high quantum yield, especially **3** and **4** have 0.93 and 0.77 respectively. This is evidently by the incorporation of highly conjugated naphthalene units. Compounds **7** and **8** with OMe phenyl exhibits 0.71 and 0.68 **ϕ** value. Pentafluoro phenyl substitution resulted in relatively lower quantum yield. In electronically excited state of the molecule charge separation over the molecules is

high; dipole moment is high and thus results in significant Stokes shift. In addition, the excitons are localized in any one of the three arms of TAA due to the conformational changes occurs in high polar medium [37]. They gain remarkable dipole moment in locally excited state.

3.2 Electrochemistry

To evaluate electrochemical behavior of the synthesized molecules cyclic voltammetry technique was used. Samples at 10^{-5} M concentration in anhydrous acetonitrile was purged with nitrogen for 10 minutes before the experiment: this reduces the interference of oxygen on redox process [38]. Experiments were carried out in 50 mV/s with tetrabutylammonium hexafluorophosphate ($TBAPF_6$) as supporting electrolyte. The instrument was calibrated with ferrocene as external standard. Using this Fc/Fc+ redox potential, HOMO and LUMO values were calculated using the formula, $E_{HOMO} = - (E_{ox} + 4.8 - E_{Fc/Fc}^{+})$ [39]. Electrochemistry of TAA is interesting because, it can transfer positive charge via radical cation [40]. All the compounds have exhibited irreversible redox peak in positive potential which corresponds to triarylamine moiety and no peaks were observed in negative potential. HOMO values lie in the range of -5.1 to -5.5 eV: compounds **3**-**6.** HOMO values are matching with most widely used hole transporting materials such as PEDOT:PSS (-5.3 eV) [41, 39] and ensures very low barrier for hole injection [42]. Peng and co-

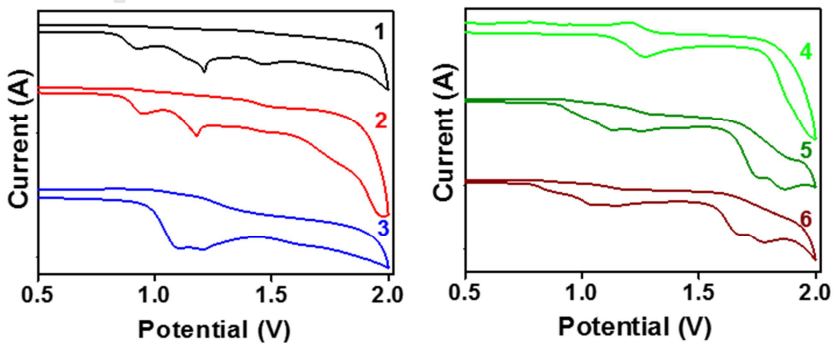

Figure 2. Cyclic voltammogram of compounds **1**-**8** in acetonitrile at 50 mV/s scan rate

workers have also reported TAA based polymers with shallow HOMO values [42]. Poly(4-butylphenyl)diphenylamine (Poly-TPD) with HOMO -5.4 eV exhibited

Table 2. HOMO, LUMO and band gap values

Comp. No	Experimental			Computational			
	HOMO[a]	LUMO	Band gap (eV)[b]	HOMO	LUMO	Bandgap (eV)[c]	
						Gaussian	VASP
1	-5.52	-2.50	3.05	-5.79	-2.03	3.76	3.21
2	-5.53	-2.25	3.28	-5.64	-2.49	3.15	3.31

mobility up to 10^{-4} cm^2 V^{-1} s^{-1} [43, 44]. Interestingly compounds **7** and **8** have HOMO level at -5.53 and -5.41 eV ensures that these compounds can be used for easy hole transport. LUMO values are obtained from the absorption edge: and band gap values are calculated [44].

3	-5.30	-2.47	2.83	-5.01	-1.75	3.25	3.46
4	-5.38	-2.46	2.92	-5.06	-1.78	3.28	3.31
5	-5.22	-2.36	2.86	-5.37	-2.14	3.23	3.67
6	-5.18	-1.89	3.29	-5.45	-2.19	3.25	3.72
7	-5.53	-2.55	2.98	-4.85	-1.57	3.27	3.21
8	-5.41	-2.55	2.86	-4.90	-1.51	3.39	3.17

[a] Calculated from E_{ox} of cyclic voltammetry
[b] Optical band gap
[c] Gaussian (B3LYP 6-31G*) & VASP (VASP GGA-PBA)

3.3 Thermal Behaviour

Thermal stability of active semiconducting material is also an important characteristics for better device performance and durability. The thermal behavior of the new compounds were studied by differential scanning calorimetry (DSC). And thermogravimetric analysis (TGA). Thermograms are given in Figures **3** and **4**. Experiments were carried out in nitrogen atmosphere at a heating rate of 5 °C per minute. In our previous works [45], we have reported formyl/nitrile substituted triarylamines with no spacer; they possess good thermal stability. Introducing an ethylene spacer improved the thermal behavior and ensures these molecules can withstand post deposition thermal annealing process to improve the film morphology. After post deposition annealing, the effectiveness in the packing of molecule in film has been found to be noticeable due to extensive pi-pi stacking.

In compound **3**, the structural change induced by the spacer has reduced the rigidity in structure and lowered the melting point. Compounds **7** and **8** exhibited the highest melting points among the compounds studied. Compounds **5** and **6** with pentafluorophenyl groups have moderate melting points. Thermogravimetric analysis have been carried out to support the thermal properties of these molecules. 10 % weight loss was observed in the range of 299-373 °C.

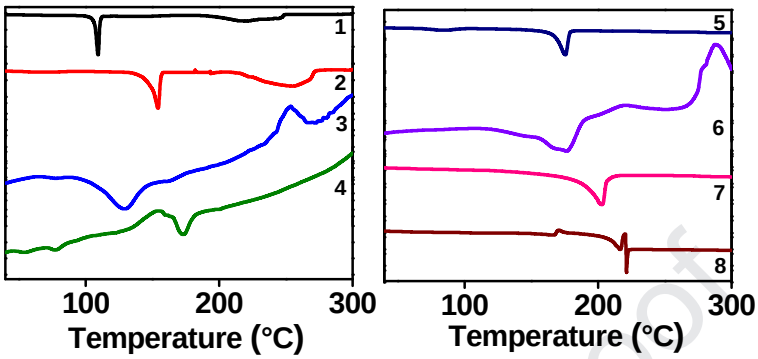

Figure 3. DSC thermogram of compounds **1-8**

235

Table 3. Thermal properties of compounds **1-8**

Compd. No.	T_m °C	T_d °C
3	127	299
4	165	373
5	177	343
6	178	315
7	205	304
8	224	366

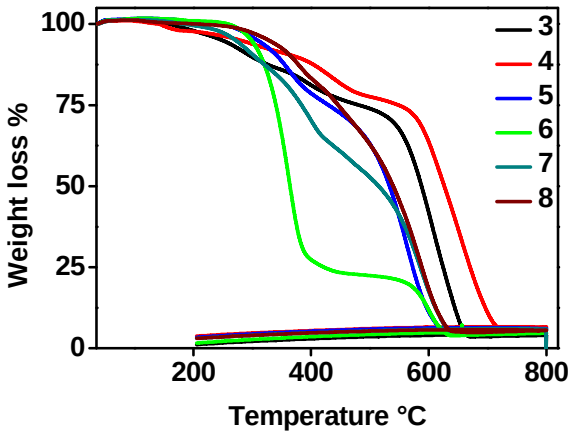

Figure 4. TGA curves of compounds **3-8**

3.4 Morphological analysis of thin films

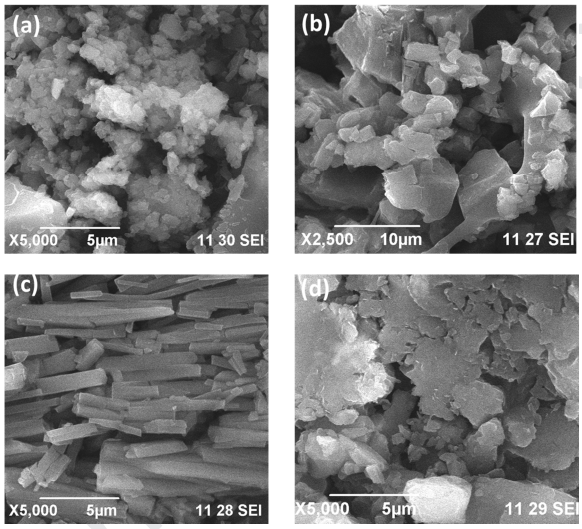

The control in the self-assembly of films casted via any solution processing technique is an important challenge for mono/multi-layered organic electronic devices. The morphology of films can be tuned by various techniques such as solvent choice, use of additives and post deposition methods [25-29].

Figure 5. Topographic images obtained by SEM for compound **3** (a), **4** (b), **7** (c), and **8** (d)

For SEM analysis, samples were dissolved in a binary mixture of toluene and chloroform (3:7) and spin coated at 3200 rpm for 45 seconds and heated to remove the residual solvent. Topography of active layer of the devices (four devices with compounds **3**, **4**, **7**, and **8)** was analyzed by SEM and shown in **Figure 5**. Compounds **3** and **4** with naphthalene substitution have shown featureless random sized clusters. Although compounds **7** and **8** are structurally similar their film topographic structures

are non-identical. Compound **7** has well defined rod like structures which are tightly packed in the defined area. Compound **8** exhibited clustered flakes of molecules. This topographical alignment of the molecules in thin film strongly supports uniform packing and ultimately ensures the higher mobility and improved charge injection [46].

3.5 Thin film X-ray diffraction analysis

Spin coated thin films are analyzed by XRD technique to support the crystallinity induced by the binary solvent system with post thermal annealing process. The optimized ratio (7:3, chloroform and toluene) only gives uniform film, whereas the other ratios and mono solvent systems produces disconnected patches.

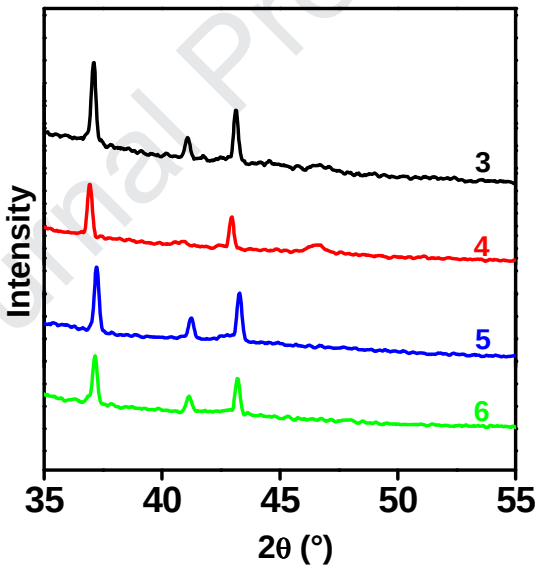

Figure 6. Thin film XRD for the compounds **3**, **4**, **7**, and **8.**

The XRD of the active layer of the four devices are given in **Figure 6**. Films made in mono solvent system produced amorphous nature. Similarly before thermal annealing process there was no significant peaks were observed. The sharp peaks at 31, 37, 43 and 47 revealed the crystalline nature of the films. Highly ordered arrangement of the donor molecules are expected to result in high hole mobility.

3.6 Computational basis

For better understanding of electronic and spectral properties, the new TAA molecules are studied through computational methods. Calculations of DFT are executed using VASP ab-initio software under MedeA Package. The Density of states (DOS) were computed by PBE functional theory to get insight into the Fermi levels. Band gap values were calculated by Gaussian and VASP methods and are given in Table 2. The negligible variation can be accounted for the additional Fermi level in crystalline structure. However, these band gap values are well in agreement with experimentally obtained values (Table 2).

Frontier molecular orbitals (FMOs) are visualized in **Figure 7**. HOMO is located over main triphenylamine moiety and LUMO is located over acceptor substituted arms. In molecules **3** & **4** and **7** & **8** (comparison with respect to substituents) only CHO group holds LUMO distribution. Molecules **5** & **6** shows LUMO only over aryl substitution side because of the pentafluoro groups. The DOS band gap values predicted by MedeA range from 1.41 eV to 2.55 eV and represented as graphs in Figure S3. The Fermi regions near the FMOs have shown good spread and signifies the possible states the charge carrier can move. In this context molecule **7** and **8** have highest possible charge carrier movement. Consequently the molecule **8** is arranged in the orthorhombic P212121 pattern in best alignment with feasible hopping distance. The shortest distance was observed along the edges of the molecule where the HOMO and LUMO were located. The DOS studies was used to calculate energy per unit volume and the calculated data are given in Table S1. The highest volume is obtained for molecule **8** and it signifies the denser packing per unit. In molecules **7** and **8**, swapping of CHO and CN group results in almost same appearance of LUMO, but **8** has more states than any other molecule in the series. The smallest gaps are found in **1** and **2**, obviously suggesting that extension of conjugation has enhanced the DOS levels.

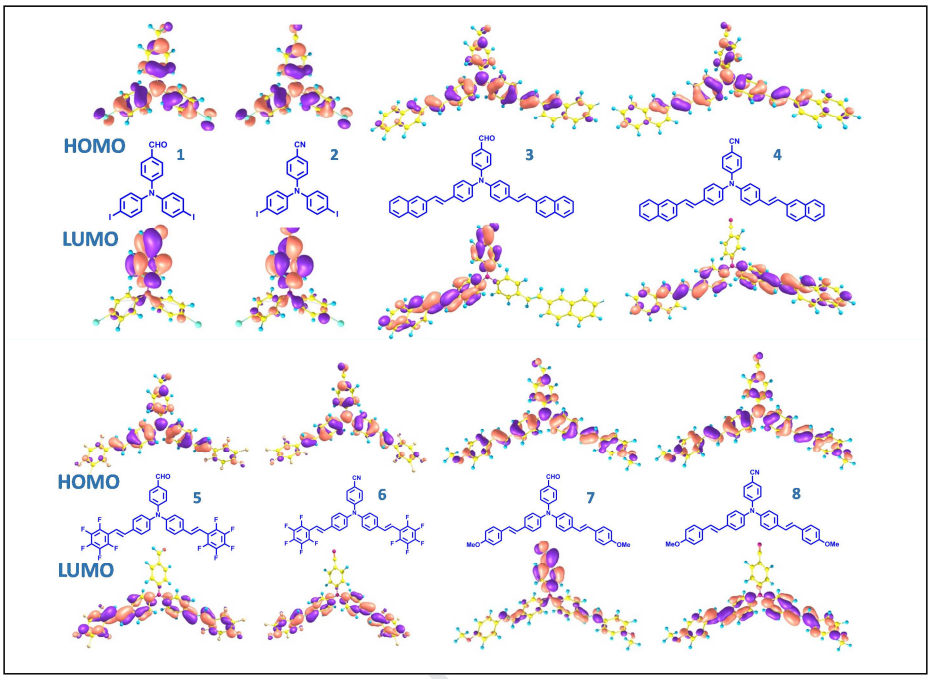

Figure 7. Frontier molecular orbitals visualized by Gaussian

3.7 OFET characteristics

Charge transport properties of the new unsymmetrical TAA were studied by OFET devices. All the solution processed BGTC devices exhibited *p* channel behavior with good transistor characteristics as shown in Figure **8**. The pre-alligned solution of compounds in the binary solvent was spin coated over thermally grown silicon dioxide layer. The solubility of compounds and misciblity of the solvents are very crucial as they define the crystallization of active layer and hole mobility. Among the six compounds studied **3**, **4**, **7**, and **8** have shown FET behaviour. Nevertheless, compounds **3** and **4** seems to be promising to possess good mobility by structure, the ethylene spacer changes the self-organzing ability of naphthalene units and they result in modest performance. The molecular packing pattern obtained from computational studies helped us to ratinalise this behaviour of compounds **3** and **4** (Figure S4). From the linear plot of the square root of drain to source current ($I_{DS}^{1/2}$) versus the gate voltage, threshold voltage (V_{TH}) and charge carrier mobility (μ) were calculated.

Mobility is extracted from the saturation regime of the transfer curve using the formula

$$\mu = \frac{2L}{CW}(Slope)^2$$

Compounds **5** and **6** failed to give FET behaviuor may be due to electron withdrawing nature of pentafluorophenyl substitution which hampers the hole flow in the molecule. Compounds **3** and **4** exhibited mobilties up to 0.01 annd 0.07 $cm^2 V^{-1}s^{-1}$ respectively, with $I_{ON/OFF}$ ratio of 10^6 and 10^5. Ultimately, methoxy substituion resulted in good OFET behaviour; might be due to the electronic effect of donating methoxy group and their mode of interactions. The mobility obtained was 1 $cm^2 V^{-1}s^{-1}$, with 10^6 on/off ratio. All the transistor charateristics are greately improved from the previously reported values for TAA based molecules [13-17]. Molecular glasses of TAA have been analysed by Sonntag and co-workers exihibited only 10^{-4} magnitude of mobility [15]. Cranivo et al [20] have reported good mobility with TAA-thiophene hybrids but $I_{on/off}$ was very low. Molecule **8** possess the best crystalline packing with 2.1 Å, 2.1 Å and 5.1 Å interatomic distance (DFT) and exhibited the higher charge carrier mobility among the molecules studied. The new TAA molecules can be utilized for various electronic application.

Table 4. OFET characteristics of ethylene bridged TAAs

Compd. No.	μ ($cm^2V^{-1}s^{-1}$)	V_{TH} (V)	$I_{ON/OFF}$
3	0.01±0.09	1	10^6
4	0.07±0.02	-16	10^5
7	0.11±0.01	-4	10^6
8	1.0±0.05	-1	10^6

*Standard deviation is calculated from five devices

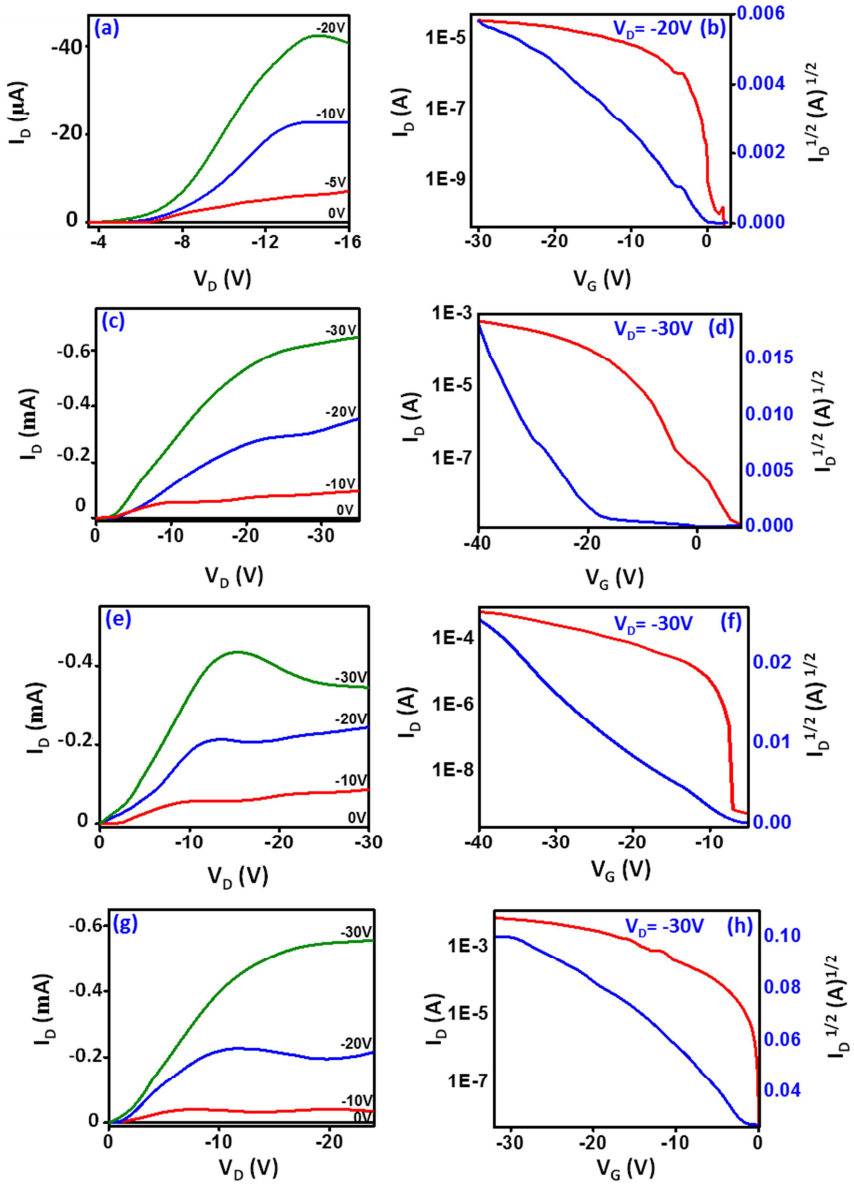

Figure 8. Output and transfer curves of compounds **3** (a, b), **4** (c, d), **7** (e, f), and **8** (g, h)

Conclusion

In summary, new butterfly type unsymmetrical triarylamines were designed and synthesised successfully by Heck coupling reaction. All the molecules exhibited HOMO values in the range of -5.1 to -5.4 eV and ensures they can be potentially employed as hole transporting and electron blocking layer for various organic electronic devices. The molecules showed good thermal stability to withstand the post deposition process at 90 °C. Thermal annealing improved the crystallinity of the thin film coated from a binary solvent system comprised of chloroform and toluene in 7:3 proportion. Among many solvents tried out, this specific ratio produced uniform film with improved the crystallinity after post thermal annealing process. Devices fabricated in bottom gated top contact (BGTC) architecture showed typical *p*-channel behaviour. Among the molecules, methoxy substituted compound **8** showed high carrier mobility up to 1 cm^2 V^{-1} s^{-1} with 10^6 $I_{ON/OFF}$ current ratio. This investigation signifies the role of new organic semiconducting *p* - channel material towards high performing OFETs and encourages their application in various electronic devices.

Acknowledgements

Financial assistance provided by the Council of Scientific & Industrial Research, New Delhi (02(0222)/14/EMR-II) is gratefully acknowledged. One of the authors (DR) thank the Central University of Tamil Nadu for a research fellowship.

Appendix I Supplementary data

Supplementary data contains detailed ^{1}H NMR, ^{13}C NMR, and HRMS spectral data and spectra of compounds; Computational studies-Density functional theory (DFT): molecule geometrical parameters at ground state, density of states graph, crystal parameters, packing pattern; Time dependent-density functional theory (TD-DFT): Electronic absorption behaviour.

References

1. S. R. Forrest, The path to ubiquitous and low-cost organic electronic appliances on plastic, Nature 428 (2004) 911-918. doi: 10.1038/nature02498.
2. H. Yan, Z. Chen, Y. Zheng, C. Newman, J. R. Quinn, F. Dotz, M. Kastler, A. Facchetti, A high-mobility electron-transporting polymer for printed transistors, Nature 457 (2009) 679-687. doi: 10.1038/nature07727.
3. X. Ji, P. Zhou, L. Zhong, A. Xu, A. C. O. Tsang, P. K. L. Chan, Smart surgical catheter for c-reactive protein sensing based on an imperceptible organic transistor, Adv. Sci. 5, (2018) 1701053-1701060, doi: 10.1002/advs.201701053.
4. J. Li, R. Bao, J. Tao, Y. Peng, C. Pan, Recent progress in flexible pressure sensor arrays: from design to applications, J. Mater. Chem. C 6 (2018)11878-11892. doi: 10.1039/c8tc02946f.
5. P. Ihalainen, M. Pesonen, P. Sund, T. Viitala, A. Maattanen, J. Sarfraz, C. E. Wilén, R. Osterbacka, J. Peltonen, Printed biotin-functionalized polythiophene films as biorecognition layers in the development of paper-based biosensors, Applied Surface Science 364 (2016) 477–483, doi: 10.1016/j.apsusc.2015.12.187.
6. H. Fana, S. Hana, Z. Songa, J. Yua, H. E. Katz, Organic field-effect transistor gas sensor based on GO/PMMA hybrid dielectric for the enhancement of sensitivity and selectivity to ammonia, Organic Electronics 67 (2019) 247–252. doi: 10.1016/j.orgel.2019.01.038.

7. W. Tang, Y. Huang, L. Han, R. Liu, Y. Su, X. Guo, F. Yan, Recent progress in printable organic field effect transistors, J. Mater. Chem. C 7 (2019) 790-808. doi 10.1039/c8tc05485a.

8. C. Bulumulla, R. Gunawardhana, R. N. Kularatne, M. E. Hill, G. T. McCandless, M. C. Biewer, M. C. Stefan, Thieno[3,2‐b]pyrrole-benzothiadiazole banana-shaped small molecules for organic field-effect transistors, ACS Appl. Mater. Interfaces 10 (2018) 11818−11825. doi: 10.1021/acsami.8b01113.

9. H. Kobayashi, N. Kobayashi, S. Hosoi, N. Koshitani, D. Murakami, R. Shirasawa, Y. Kudo, D. Hobara, Y. Tokita, M. Itabashi, Hopping and band mobilities of pentacene, rubrene, and 2,7-dioctyl[1]benzothieno[3,2-b][1]benzothiophene (C8-BTBT) from first principle calculations, The Journal of Chemical Physics 139 (2013) 014707, doi: 10.1063/1.4812389.

10. Y. Yuan, G. Giri, A. L. Ayzner, A. P. Zoombelt, S. C. B. Mannsfeld, J. Chen, D. Nordlund, M. F. Toney, J. Huang & Z. Bao, Nature Communications 5:3005 (2013) 1-9, doi: 10.1038/ncomms4005.

11. H. Minemawari, T. Yamada, H. Matsui, J. Tsutsumi, S. Haas, R. Chiba, R. Kumai, T. Hasegawa, Inkjet printing of single-crystal films, Nature, 475 (2011) 364-367, doi: 10.1038/nature10313.

12. T. Leydecker, D. T. Duong, A. Salleo, E. Orgiu, P. Samorì, Solution-processed field-effect transistors based on dihexylquaterthiophene films with performances exceeding those of vacuum-sublimed films, ACS Appl. Mater. Interfaces 6 (2014) 21248 −21255, doi: 10.1021/am506245v.

13. A. Cravino, S. Roquet, O. Aleveque, P. Leriche, P. Frere, J. Roncali, Triphenylamine-oligothiophene conjugated systems as organic semiconductors for opto-electronics. Chem. Mater. 2006 18 2584-2590 doi: 10.1021/cm060257h.

14. P. Devibala, R. Dheepika, P. Vadivelu, S. Nagarajan, Synthesis of aroylbenzoate-based push-pull molecules for ofet applications, ChemistrySelect 4, (2019) 2339 - 2346, doi: 10.1002/slct.201803394.

15. M. Sonntag, K. Kreger, D. Hanft, P. Strohrieg, Novel star-shaped triphenylamine-based molecular glasses and their use in OFETs, Chem. Mater. 2005 17 3031-3039, doi: 10.1021/cm047750i.
16. Y. Song, C. Di, W. Xu, Y. Liu, D. Zhanga D. Zhu, New semiconductors based on triphenylamine with macrocyclic architecture: synthesis, properties and applications in OFETs, J. Mater. Chem., 17 (2007) 4483–4491, doi: 10.1039/b708887f.
17. T. P.I. Saragi, T. F. Lieker, J. Salbeck, High ON/OFF ratio and stability of amorphous organic field-effect transistors based on spiro-linked compounds, Synthetic Metals 148 (2005) 267–270, doi: 10.1016/j.synthmet.2004.10.007.
18. J. Wang, K. Liu, L Ma, X. Zhan, Triarylamine: versatile platform for organic, dye-sensitized, and perovskite solar cells, Chem. Rev. 116 (2016) 14675 −14725, doi: 10.1021/acs.chemrev.6b00432.
19. Y. Song, C. Di, X. Yang, S. Li, W. Xu, Y. Liu, L. Yang, Z. Shuai, D. Zhang, D. Zhu, A cyclic triphenylamine dimer for organic field-effect transistors with high performance, J. Am. chem. Soc. 128 (2006) 15940-1594, doi: 10.1021/ja064726s.
20. B. H. A. Becerri, M. E. Roberts, Z. Liu, J. Locklin, Z. Bao, High-performance organic thin-film transistors through solution-sheared deposition of small-molecule organic semiconductors, Adv. Mater. 20 (2008) 2588–2594, doi: 10.1002/adma.200703120.
21. W. Y. Lee, J. H. Oh , S.L. Suraru, W. C. Chen, F. Wurthner , Z. Bao, High-mobility air-stable solution-shear-processed n-channel organic transistors based on core-chlorinated naphthalene diimides, Adv. Funct. Mater. 21 (2011) 4173–4181, doi: 10.1002/adfm.201101606.
22. I. Zergioti, M. Makrygianni, P. Dimitrakis, P. Normand, S. Chatzandroulis, Laser printing of polythiophene for organic electronics, Applied Surface Science 257 (2011) 5148–5151, doi: 10.1016/j.apsusc.2010.10.145.
23. J. Rivnay, L. H. Jimison, J. E. Northrup, M. F. Toney, R. Noriega, S. Lu, T. J. Marks, A. Facchetti, A. Salleo, Large modulation of carrier transport by grain-boundary molecular packing and microstructure in organic thin films, Nature materials, 8 (2009) 952-959, doi: 10.1038/NMAT2570.

24. D. Bharti, S. P. Tiwari, Crystallinity and performance improvement in solution processed organic field-effect transistors due to structural dissimilarity of the additive solvent, Synthetic Metals 215 (2016) 1–6, doi: 10.1016/j.synthmet.2016.01.013.

25. J. W. Jeong, G. Jo, S. Choi, Y. A. Kim, H. Yoon, S. W. Ryu, J. Jung, M. Chang, Solvent additive-assisted anisotropic assembly and enhanced charge transport of π⍰ conjugated polymer thin films, ACS Appl. Mater. Interfaces 10 (2018) 18131−18140, doi: 10.1021/acsami.8b03221.

26. C. Bao, M. Kaur, W. S. Kim, Toward a highly selective artificial saliva sensor using printed hybrid field effect transistors, Sensors & Actuators: B. Chemical 285 (2019) 186–192, doi: 10.1016/j.snb.2019.01.062.

27. D. Bharti, V. Raghuwanshi, I. Varun, A. K. Mahato, S. P. Tiwari, Directional solvent vapor annealing for crystal alignment in solution processed organic semiconductors, ACS Appl. Mater. Interfaces, 9 (2017) 26226–26233, doi: 10.1021/acsami.7b03432.

28. Z. Tao, T. M. Brahim, W. Lei, M. Harnois, E. Jacques, Impact of the post-thermal annealing on OFETs using printed contacts, printed organic gate insulator and evaporated C60 active layer, Solid-State Electronics 150 (2018) 51-59 doi: 10.1016/j.sse.2018.10.011.

29. F. Dinellia, M. Murgiaa, F. Biscarini, D.M. De Leeuw, Thermal annealing effects on morphology and electrical response in ultrathin film organic transistors Synthetic Metals 146 (2004) 373–376, doi: 10.1016/j.synthmet.2004.08.016.

30. C. Quinton, V. A. Rizzo, C. D. Verdes, F. Miomandre and P. Audebert. Electrochimica Acta 110 (2013) 693-701, doi: 10.1016/j.electacta.2013.02.113.

31. J. K Augustine, A. Bombrun, R. N. Atta, A practical and cost-efficient, one-pot conversion of aldehydes into nitriles mediated by ‘activated DMSO’, Synlett 5 (2011) 2223–2227, doi: 10.1055/s-0030-1261181.

32. A. R. Aiyar, J. Hong, J. Izumi, D. Choi, N. Kleinhenz, E. Reichmanis, Ultrasound-induced ordering in poly(3-hexylthiophene): role of molecular

and process parameters on morphology and charge transport, ACS Appl. Mater. Interfaces 5 (2013) 2368-2377, doi: 10.1021/am3027822.

33. D. Peckus, T. Matulaitis, M. Franckevius, V. Mimait, T. Tamulevius, J. Simokaitiene, D. Volyniuk, V. Gulbinas, S. Tamulevicius, J. V. Grazulevicius, Twisted intramolecular charge transfer states in trinary star-shaped triphenylamine-based compounds J. Phys. Chem. A, 122 (2018) 3218, doi: 10.1021/acs.jpca.8b00981
34. J. Tagarea, D. Kumar, J. H. Joub, S. Vaidyanathan, Synthesis, photophysical, theoretical and electroluminescence study of triphenylamine-imidazole based blue fluorophores for solution-processed organic light emitting diodes. Dyes pigm 160 (2019) 944–956, doi: 10.1016/j.dyepig.2018.09.007.
35. J. Duan, H. Pan, C. Wei, J. Xiao, G. Zhaia, W. Su, Synthesis and physical properties of triphenylamine-functionalized twistacenes: blueemitting fluorophores, RSC Adv. 7 (2017) 10570, doi: 10.1039/c6ra28814f
36. N. A. Montgomery, J. C. Denis, S. Schumacher, A. Ruseckas, P. J. Skabara, A. Kanibolotsky, M. J. Paterson, I. Galbraith, G. A. Turnbull, D. W. Samuel, Optical excitations in star-shaped fluorene molecules, J. Phys. Chem. A 115 (2011) 2913–2919, doi: 10.1021/jp1109042.
37. F. Terenziani, C. Sissa, A. Painelli, Symmetry breaking in octupolar chromophores: solvatochromism and electroabsorption, J. Phys. Chem. B 112 (2008) 5079-5087 doi: 10.1021/jp710241g.
38. N. Elgrishi,́ K. J. Rountree, B. D. McCarthy, E. S. Rountree, T. T. Eisenhart, J. L. Dempsey, A practical beginner' s guide to cyclic voltammetry, J. Chem. Educ. 95 (2018) 197 −206, doi: 10.1021/acs.jchemed.7b00361.
39. Z. Li, T. Ye, S. Tang, C. Wang, D. Ma and Z. Li, Triphenylamine-based π-conjugated dendrimers: convenient synthesis, easy solution processability, and good hole-transporting property, J. Mater. Chem. C, 3 (2015) 2016-2023, doi: 10.1039/C4TC01923G.
40. S. J. Yeh, C. Y. Tsai, C. Y. Huang, G. S. Liou, S. H. Cheng, Electrochemical characterization of small organic hole-transport molecules based on the triphenylamine unit, Electrochemistry Communications, 5 (2003) 373–377, doi: 10.1016/S1388-2481(03)00072-9.

41. X. Zhao, M. Wang, Organic hole-transporting materials for efficient perovskite solar cells, Materials Today Energy, 7 (2018) 208-220, doi:10.1016/j.mtener.2017.09.011.
42. W. Yang, F. Peng, J. Xu, Y. Zhang, R. He and Y. Cao, Ether-soluble hole-transporting polymers based on triphenylamine/phenothiazine moiety with shallow HOMO level, Polym. Chem., 10 (2019) 1367-1376 doi: 10.1039/C8PY01677A.
43. N. Li, Z. Fan, H. Zhao, Y. Quan, Q. Chen, S. Ye, S. Li, Q. Fan, W. Huang, A bipolar macrospirocyclic oligomer based on triphenylamine and 4,5-diazafluorene as a solution-processable host for blue phosphorescent organic light-emitting diodes, Dyes Pigm. 134 (2016) 348-357, doi: 10.1016/j.dyepig.2016.06.003.
44. X. Liu, X. Ding, Y. Ren, Y. Yang, Y. Ding, X. Liu, A. Alsaedi, T. Hayat, J. Yao, S. Dai, A star-shaped carbazole-based hole-transporting material with triphenylamine side arms for perovskite solar cells, J. Mater. Chem. C., 6 (2018) 12912, doi: 10.1039/c8tc04191a.
45. R. Dheepika, S. Sonalin, P. M. Imran, S. Nagarajan, Unsymmetrical starburst triarylamines: synthesis, properties, and characteristics of OFETs, J. Mater. Chem. C., 6 (2018) 6916 doi: 10.1039/c8tc02017e.
46. J. C. S. Costa, L. M. N. B. F. Santos, Hole transport materials based thin films: topographic structures and phase transition thermodynamics of triphenylamine derivatives, J. Phys. Chem. C., 117 (2013) 10919-10928, doi: 10.1021/jp4002274.

Highlights

- New functionalized triarylamines are designed, synthesised and scrutinised for OFET applications.
- HOMO level (5.2 to 5.4 eV) ensures efficient hole injection and transport.
- Band gap tuned with respect to the electron donating and withdrawing substituents.
- OFETs with bottom gate top contact architecture is fabricated by spin coating from a binary solvent mixture.
- Exhibited higher melting points ensures the device durability with higher mobility up to 1 $cm^2 V^{-1} s^{-1}$ with 10^6 $I_{on/off}$ current ratio.